Supplement of Atmos. Chem. Phys., 14, 8533–8557, 2014
http://www.atmos-chem-phys.net/14/8533/2014/
doi:10.5194/acp-14-8533-2014-supplement

Atmospheric Chemistry and Physics Open Access

Supplement of

Uncertainties in assessing the environmental impact of amine emissions from a CO_2 capture plant

M. Karl et al.

Correspondence to: M. Karl (mka@nilu.no)

S1. Gridded emissions in the EMEP model

The standard emissions input to the EMEP model is gridded national annual emissions of sulphur oxides (95% as SO_2 and 5% as particulate SO_4), nitrogen oxides (NO_x = NO + NO_2), ammonia (NH_3), non-methane volatile organic compounds (NMVOC), carbon monoxide (CO), and particulates ($PM_{2.5}$, PM_{10}) (http://www.ceip.at). The traditional EMEP model has a spatial resolution of 50 km, but here we have used an emission inventory based on TNO-MACC (Kuenen et al., 2011) with spatial resolution of 1/8 × 1/16 lon-lat (approximately 7 × 7 km^2), rescaled to match the official EMEP 2009 country total emissions. The dataset, hereafter denoted TNO7, was delivered by INERIS for the "TFMM Scale Dependency Study" (Schaap et al., 2012). Details of the treatment of such emissions in the EMEP model (including speciation, time-variation, etc.) are given in Simpson et al. (2012). Even these TNO7 emissions have coarser resolution compared to the 2 × 2 km^2 model grid. In order to make the power plant emission as realistic as possible, the TNO7 data were first reallocated to a finer 2 km grid, with similar projection and size as the inner model domain. Next, the redistributed emissions in approximately 10 km distance from Mongstad were replaced by representative background values, whereas the excess emission was reallocated to the single 2 × 2 km^2 grid enclosing the Mongstad refinery and the power plant.

Total NO_x area emission in the grid cell of Mongstad was 260 Mg per year (SNAP category 1: Combustion in energy and transformation industries). The total NO_x emission in the Mongstad grid cell from area and point sources for the year 2007 was reported by Statoil Mongstad to be 1930 Mg yr^{-1} as registered in the European Pollutant Release and Transfer Register (http://prtr.ec.europa.eu). The contribution from the power plant is estimated to be 140 Mg yr^{-1} based on data by Statoil Mongstad for 2007 (see **Table S3**). It is assumed that the installation of the CCP does not affect the NO_x emissions of the power plant.

S2. Plume rise treatment in the EMEP model

Three options for plume rise calculation for point sources have been implemented into the EMEP model. The option 'NILU plume' takes into account different boundary layer stability conditions, where the inverse Obukhov length is used to characterize the boundary layer stability, and follows the plume rise description by Briggs (e.g. Briggs, 1971) with modifications. The option 'ASME Plume' is adequate for buoyant plumes and calculates final plume rise for neutral and stable conditions using a simplified parameterization, with exhaust gas volume flow rate as main control parameter (ASME 1973; Seinfeld and Pandis, 1998). The option 'PVDI Plume' is adequate for large point sources and calculates plume rise according to the German VDI Guideline 3782 Part 3 (VDI, 1985) considering parameterizations for different temperature stratifications and heat fluxes based on plume rise equations by Briggs (1971) with modifications for neutral temperature stratification (Pregger and Friedrich, 2009). Emitted heat flux (in MW) is the main control parameter in the 'PVDI Plume' parameterization, which is proportional to exhaust gas volume flow rate and temperature difference between exhaust gas and ambient air temperature.

Final plume rise (Δh_f) calculated by the three plume rise methods was compared for a generic stack with exhaust gas temperature of 313.15 K and ambient air temperature of 283.15 K. Three test series were performed: (1) variation of stack height (*Hs*) between 50 and 90 m; (2) variation of exit velocity (*Vs*) between 5 and 13 m s^{-1}; and (3) variation of diameter (*D*) between 2.5 and 6.5 m. For 'NILU Plume', a stable condition (L = 20 m), an unstable condition (L = -10 m) and a neutral condition ($L = 10^6$ m) were tested. For 'ASME Plume' both a stable condition (dT/dz = 0.10 K m^{-1}) and a neutral condition (dT/dz = -0.01 K m^{-1}) were tested. **Table S4** summarizes the final plume rise results obtained from this test. For all tested parameter sets, 'NILU Plume' resulted in the lowest plume rise. The low final plume rise of the 'NILU Plume' parameterization can be explained by the decision flow of the plume rise algorithm - illustrated in **Figure S1** - which tends to select low values for final plume rise. For example, the lower of the stable momentum rise and neutral-unstable momentum rise is chosen as final plume rise. 'ASME Plume' results were within a factor of 2 similar to the 'NILU Plume' results for stable condition, but up to 8 times higher than the 'NILU Plume' results for neutral condition. For the given ranges of variation, calculated final plume rise was most sensitive to changes in stack diameter. 'ASME Plume' for neutral condition gave the highest plume rise (147 m) in the test, for the largest diameter D = 6.5 m. For the stack configuration of this study (*Hs* = 60 m, D = 7.14 m, *Vs* = 10 m s^{-1}) 'ASME Plume' (neutral) and 'PVDI Plume' gave similar results, with final plume rise of about 220 m.

We have tested the sensitivity of the ground-level maximum concentration within 8 km downwind of the source by implementing the plume rise schemes of our work ('NILU Plume', 'PVDI Plume', and 'ASME Plume') in a Gaussian plume model. The assumption in the Gaussian plume model included: flat terrain (appropriate for Mongstad within a radius of 8 km),

mixing height of 1000 m, no effect of buildings (as in the EMEP model), and no stack downwash. Tests were done for three typical situations in the atmospheric boundary layer: neutral case with wind speed u = 5 m s^{-1}, moderately stable case with u = 3 m s^{-1}, and unstable case with u = 2 m s^{-1} (see **Figure S2**).

For neutral conditions the result was a wide area with ground-level concentrations between 100 and 400 ng m^{-3} (1000 - 4500 m downwind the source). Effective emission height for 'NILU Plume', 'PVDI Plume', and 'ASME Plume' was 139 m, 169 m, and 177 m, respectively. Since maximum ground level concentration (C_{max}) is roughly proportional to the square of the effective emission height, the increase from 140 m to 180 m implies a potential decreasing C_{max} by 40%. This corresponds well with the result for the neutral case: C_{max} in the 'NILU Plume' calculation is roughly twice as high as for the other two plume rise schemes. For 'PVDI' and 'ASME', the location of C_{max} is shifted by about 1000 m in downwind direction compared to 'NILU Plume'.

For moderately stable conditions, C_{max} is found in the largest distance from the source. Effective emission height for 'NILU Plume', 'PVDI Plume', and 'ASME Plume' was 141 m, 242 m, and 162 m, respectively. The parameterization of 'PVDI Plume' has been derived for neutral conditions and does not take in account the variation of atmospheric stability. The application of 'PVDI Plume' in moderately stable conditions resulted in very low C_{max}, which occurs in 5500 m distance from the source. For the other two plume rise schemes, high ground-level concentrations are located between 2000 m and 5000 m downwind from the source.

For unstable conditions, all schemes give similar effective emission heights (range: 290 - 330 m). C_{max} (range: 100 - 150 ng m^{-3}) is located rather close to the source, in ca. 1500 m distance. The occurrence of unstable conditions could therefore explain the high near-source concentrations of amines found in the simulations with WRF-EMEP.

S3. Evaluation of horizontal dispersion in the EMEP model

The physical processes to be modelled as diffusion in chemical transport models are different in different scales. By definition, diffusion processes are sub-grid mixing processes not resolved by the given resolution of the model. Therefore, the horizontal diffusion coefficient, which is a measure of the strength of the atmospheric turbulence, will depend on the grid resolution. For large grid cells (50×50 km^2 or 150×150 km^2) the numerical diffusion will usually be much larger than the physical diffusion at these scales. Therefore no additional diffusion term for the horizontal dispersion has been included in the EMEP model when using a 50-km grid resolution (see Simpson et al., 2012). At higher resolution scales, however, the physical diffusion will gradually become more important than numerical diffusion, and becomes greater than numerical diffusion for 5×5 km^2 cells or smaller grid cells.

In the inner domain of the WRF-EMEP model system, the distance between the midpoints of two neighbouring cells in the inner nest is 2000 m. Horizontal dispersion sigma parameters calculated according to Pasquill-Gifford show that sigma in horizontal direction is about 400 m for a 2-km resolution grid (one-sided diffusion) for unstable conditions. The sigma values are much lower (about 100 m) for neutral or more stable conditions. Thus the error introduced by neglecting horizontal diffusion under convective conditions at this scale could be up to 400/2000, corresponding to 20%. Taking into account horizontal diffusion is expected to result in a wider plume and a decrease of the maximum ground-level concentration in the plume centreline.

In order to estimate the error related to neglecting horizontal diffusion in the inner domain for WRF-EMEP simulations, we performed a test for dispersion in horizontal direction with the Eulerian model EPISODE (Walker et al., 1999; Slørdal et al., 2003). In both EMEP and EPISODE, the numerical solution of the advection terms is based upon the scheme of Bott; the fourth order scheme is utilized in the horizontal directions. The Bott scheme intends to reduce the numerical diffusion. However even at fine scales there might still be some numerical diffusion, depending on how well the plume is delimited in space and on the wind fields (Courant number). In the applied version of EPISODE all operators can be turned on or off for testing purposes.

The test was done for the horizontal dispersion from a 2000 m wide volume source (emission of an inert tracer with 1 g s^{-1}) on a 2-km resolution grid with layer height of 90 m. We used unstable conditions (ambient temperature gradient $dT/dz = -0.02$ K m^{-1}), a mixing layer height of 1000 m, and a constant horizontal wind from 45 degrees with wind speed $u = 3$ m s^{-1}. The first run considered only transport by horizontal advection while the second run considered both horizontal advection and diffusion (see **Figure S3**). Only in a distance of more than 20 km downwind from the source, significant differences of the horizontal dispersion of the plume became apparent. In 9 km distance, the ground-level concentration was reduced by 12% in the plume centreline and by 2-6% in the adjacent cells, when including horizontal diffusion. In 20

km distance, the ground-level concentration was reduced by 20% in the plume centreline and by 10-12% in the adjacent cells, when including horizontal diffusion.

In WRF-EMEP simulations, maximum ground-level concentrations of amines were always found within a radius of 10 km distance from the source (Mongstad CCP). We therefore conclude that our modelled maximum amine concentrations are at most 15% higher than they would be with physical diffusion included.

S4. Comparison of WRF meteorology to met station data

The WRF model was initialized with two datasets of meteorological initial and boundary conditions: ECMWF reanalysis data and NCEP FNL global analysis data. WRF model with both initializations was compared to local meteorological observation data in the region of Bergen at the West coast of Norway.

Comparison of wind roses for the stations Fedje, Bergen-Florida, Takle, Kvamskogen and Flesland for year 2007 in general shows good agreement between the WRF model (based on NCEP FNL data and on ECMWF data) and observations. Wind roses generated from the two model datasets were quite similar both in terms of frequency of wind direction and magnitude of wind speed. As an example, **Figure S4a - c** shows the annual wind rose based on measured data, WRF model with ECMWF data, and WRF model with NCEP FNL data at Fedje station, an island 18 km to the West of Mongstad. At Takle station (61.03ºN; 5.39ºE; 38 m a.s.l.), the WRF model for both NCEP FNL and ECMWF data overestimated the frequency of winds from southerly directions. The wind rose at the Norwegian west coast in the Bergen region changes throughout the year, with a clear prevalence of E-SE winds in winter and a higher frequency of NW winds in summer (**Fig. S4d-f**). During autumn and spring the components from SE to N are more frequent, with prevailing Atlantic winds.

The pattern of wind direction and wind speed throughout the year is reproduced at the stations Bergen, Takle, Fedje and Kvamskogen well by the WRF model (**Figure S5**). At Fedje, which is frequently exposed to strong winds, even high wind speeds were captured well. WRF tended to underestimate the wind speed of the strong winds with measured wind speed >10 m s^{-1}. On the other hand, WRF overestimated wind speeds at the inland site Kvamskogen, although it captured the pattern reasonably well. Unfortunately, none of these stations is exactly representative for the conditions at the location of the Mongstad refinery.

On the basis of daily averages, the agreement between observed temperature and modelled temperature was excellent at the stations Fedje, Flesland, Kvamskogen, and Takle, both in terms of variation and in terms of absolute values (**Figure S6**). The WRF model was capable of accurately reproducing ground air temperatures and temperature variations in the region of Mongstad during 2007. Modelled daily and monthly average temperature from the two meteorological datasets - ECMWF and NCEP FNL - was in close agreement, not deviating by more than 1°C at the four stations.

Table S1: Physiochemical characteristics of the nitrosamine and the two nitramines for which the Fugacity III model was applied. The procedure to obtain the data is adopted from the report by Yiannoukas (2011). Degradation rates DT50 (degradation time for 50% of the substance, here values refer to ultimate degradation) in water, soil, sediment and air were derived from EPISuite^{TM}, in accordance with US EPA standard methodology (US EPA, 2012).
MW: molecular weight; Kow: octanol-water partition coefficient; Koc: organic carbon partition coefficient between liquid and solid phases.

Compound group	MW ($g\ mol^{-1}$)	Water sol. ($mg\ l^{-1}$)	Vapor press. (mm Hg)	Melt point (°C)	Log Kow	Koc ($l\ kg^{-1}$)	DT50 water days	DT50 soil days	DT50 sedim. days	DT50 atmos. days
Nitrosamine-2 (NDMA) Nitrosodimethyl amine	74	$1x10^6$	2.7	25	-0.57	0.110	23	38	207	4.2
Nitramine-1 Methyl-nitramine	76	$1x10^6$	6.99	38	-1.51	0.013	15	30	135	8.5
Nitramine-2 N,N dimethyl-nitramine	90	$1x10^6$	0.361	58	-0.52	0.124	15	30	135	2.8

Table S2: Physical parameters for the generic soil and lake used in the simulations for which the Fugacity III model was applied. MTC: mass transfer coefficient.

	Units	**Value**
Catchment parameters		
Area (ex. lake)	km^2	1.95
Mean soil depth	m	10
Soil organic C	g/g	0.14
Runoff parameters		
Discharge	m/yr	1.7
Suspended particles	%vol	0.0005
Susp. particles organic C	g/g	0.14
Lake parameters		
Area	km^2	0.16
Mean depth	m	10
Volume	mill. m^3	1.6
Water retention time	yr	0.45
Sediment organic C	g/g	0.028
Transport velocities		
Air side air-water MTC	m/yr	43800
Water side air-water MTC	m/yr	438
Rain rate	m/yr	1.9
Aerosol dry deposition velocity	m/yr	0.000005256
Soil air phase diffusion MTC	m/yr	175.2
Soil water phase diffusion MTC	m/yr	0.0876
Soil air boundary layer MTC	m/yr	43800
Sediment-water MTC	m/yr	0.0876
Sediment deposition velocity	m/yr	0.00438
Sediment resuspension velocity	m/yr	0.001752
Soil water runoff rate	m/yr	1.7
Soil solids runoff rate	m/yr	0.0005256

Table S3: NO_x emissions (in Mg per year) at Mongstad in the EMEP model.

Source	**Refinery combustion (Area source)**	**Refinery (Point source, 103m stack)**	**Refinery (Point source, 50m stack)**	**CCP and power plant (Point source)**	**Total (w/o CCP)**	**Total (w CCP)**
NO_x emission (Mg per year)	260	940	590	140	1790	1930

Table S4: Final plume rise, Δh, (in m) calculated using the three plume rise options available in the EMEP model: 'NILU Plume', 'ASME Plume' and 'PVDI Plume' for exhaust gas temperature of 313.15 K, air temperature of 283.15 K, and wind speed of 2.5 m s^{-1}.

Stack configuration	**NILU Plume *neutral***	**NILU Plume *unstable***	**NILU Plume *stable***	**ASME Plume *stable***	**ASME Plume *neutral***	**PVDI Plume**
Hs=90 m, D=2.5 m, Vs=5 m s^{-1}	15	15	15	27	115	35
Hs=70 m, D=2.5 m, Vs=5 m s^{-1}	15	15	15	27	97	35
Hs=50 m, D=2.5 m, Vs=13 m s^{-1}	39	39	39	38	107	64
Hs=50 m, D=2.5 m, Vs=11 m s^{-1}	33	33	33	36	101	57
Hs=50 m, D=2.5 m, Vs=9 m s^{-1}	27	27	27	33	95	49
Hs=50 m, D=2.5 m, Vs=7 m s^{-1}	23	23	21	31	87	40
Hs=50 m, D=6.5 m, Vs=5 m s^{-1}	54	53	39	52	147	129
Hs=50 m, D=5.5 m, Vs=5 m s^{-1}	45	44	33	46	132	102
Hs=50 m, D=4.5 m, Vs=5 m s^{-1}	36	36	27	41	115	76
Hs=50 m, D=3.5 m, Vs=5 m s^{-1}	26	26	21	34	97	52
Hs=50 m, D=2.5 m, Vs=5 m s^{-1}	18	18	17	27	78	35
Hs=60 m, D=7.14 m, Vs=10 m s^{-1}	86	86	86	69	223	218

Table S5: Henry's Law coefficients for the aqueous phase partitioning in the EMEP model.

Compound	**Chemical name**	**H (mol kg^{-1} atm^{-1})**	**Reference**
MEA	2-aminoethanol	6.18×10^{6}	Ge et al. (2011)
MEA-nitramine	2-nitro aminoethanol	1.42×10^{7}	EPI Suite, Bond method
DEYA	Diethylamine	132	Ge et al. (2011)
DEYA-nitramine	N-nitro diethylamine	178	EPI Suite, Bond method
DEYA-nitrosamine	N-nitroso diethylamine	275	Mirvish et al. (1976)

Table S6: Geographical location, availability and frequency of meteorological observations at the met stations in the Bergen region.

Station/ WMO no.	**Station Name / County**	**Latitude Longitude Altitude**	**Observations**			
			Wind	**Temp.**	**RH**	**Precip.**
52535 / 307	**Fedje** / Hordaland	60.780, 4.720, 19 m	6 h	6 h	6 h	
50310 / 327	**Kvamskogen** Jonshøgdi / Hordaland	60.389, 5.964, 455 m	6 h	6 h	6 h	
50540 / 317	**Bergen**-Florida / Hordaland	60.383, 5.334, 12 m	6 h	6 h	6 h	12 h
50500 / 311	**Flesland**/ Hordaland	60.289, 5.227, 48 m	6 h	6 h	6 h	12 h
52860 / 319	**Takle** / Sogn i Fjordane	61.027, 5.385, 38 m	6 h *	6 h *	6 h *	12 h
52290 / 325	**Modalen** II / Hordaland	60.841, 5.953, 114 m	6 h *	6 h *	6 h *	12 h
56400	**Yttre** Solund / Sogn og Fjordane	61.005, 4.676, 3 m				24 h
56320	**Lavik** / Sogn og Fjordane	61.112, 5.547, 31 m				24 h
52930	**Brekke** / Sogn og Fjordane	60.959, 5.427, 240 m				24 h
52601	**Haukeland**-Storevatn / Hordaland	60.835, 5.583, 325 m				24 h
52750	**Frøyset** / Hordaland	60.848, 5.217, 13 m				24 h
52400	**Eikanger**-Myr / Hordaland	60.623, 5.381, 72 m				24 h

* Only monitored at 7, 13, 19 GMT.

Table S7: Comparison of maximum monthly values of mean air concentration, dry deposition and wet deposition of an inert tracer (emission of 1 g/s) in a 40 × 40 km^2 domain around Mongstad computed by the TAPM model and by the WRF-EMEP model (using ECMWF meteorology).

Month in 2007	Air Concentration Max. value (in 40x40 km^2) unit: ng/m^3		Dry Deposition Max. value (in 40x40 km^2) unit: mg/m^2		Wet Deposition Max. value (in 40x40 km^2) unit: mg/m^2	
	WRF-EMEP	TAPM	WRF-EMEP	TAPM	WRF-EMEP	TAPM
January	33	34	0.92	1.12	1.7	2.7
February	127	84	3.11	0.09	1.3	2.4
March	86	43	1.57	0.17	1.5	2.2
April	41	39	2.19	0.20	1.2	3.2
May	56	60	2.37	0.32	0.7	2.7
June	144	144	4.75	0.28	0.3	3.5
July	86	48	2.73	0.43	2.1	6.0
August	38	45	2.36	0.34	0.7	3.4
September	23	33	2.17	0.19	1.1	3.1
October	41	112	2.51	0.11	1.5	4.0
November	90	63	2.39	0.09	1.3	3.7
December	68	74	3.57	0.87	1.3	3.1

Both models used the following stack characteristics. Stack height: 60 m, stack diameter: 7.14 m, exit velocity: 10 m/s, and exhaust gas temperature: 313 K. Emission of inert tracer at 1 g s^{-1}.

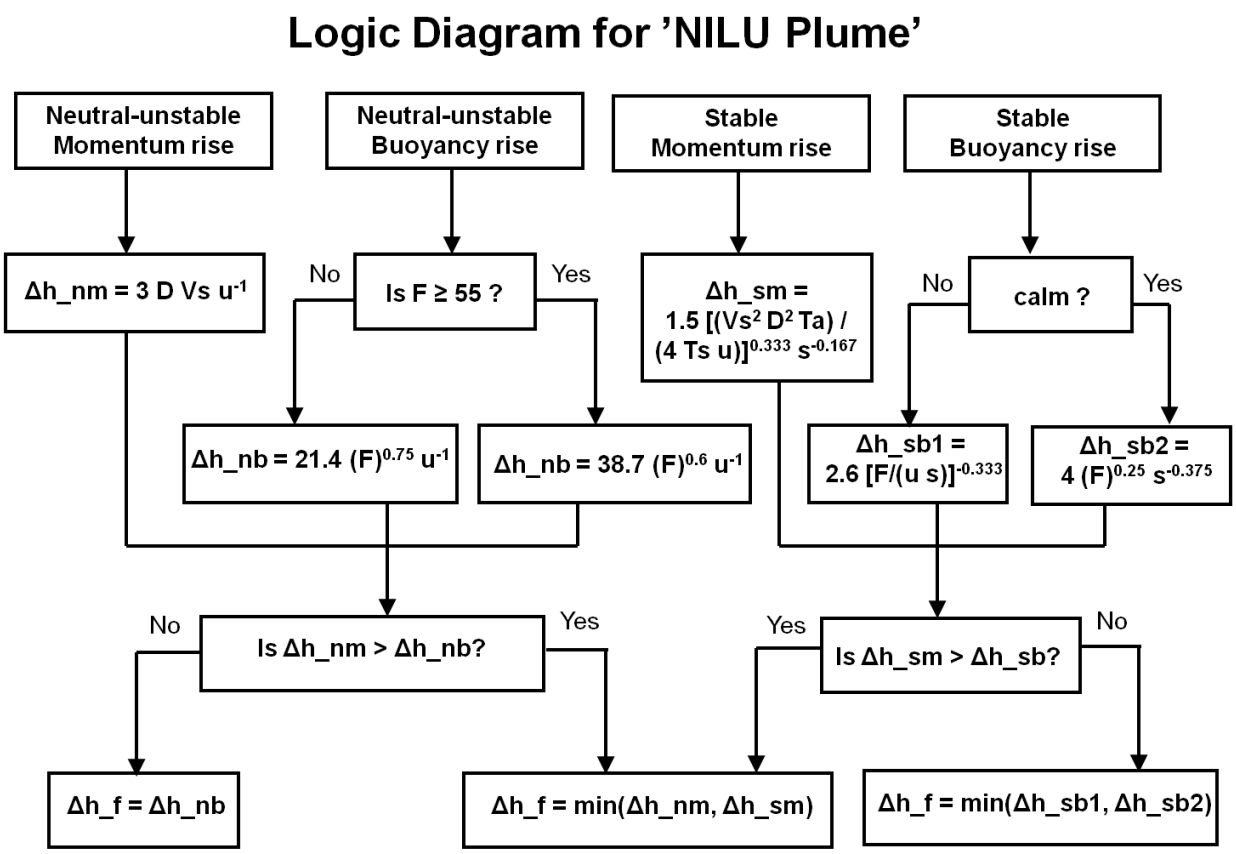

Figure S1: Logic diagram of the 'NILU Plume' algorithm to obtain final plume rise. In the diagram, F is the buoyancy factor (in m^4 s^{-3}), Vs is stack exit velocity (in m s^{-1}), D is stack diameter (in m), Ta is ambient temperature (in K), Ts is exhaust gas temperature (in K), u is wind speed at actual stack height (in m s^{-1}), and s is the stability parameter (in s^{-2}).

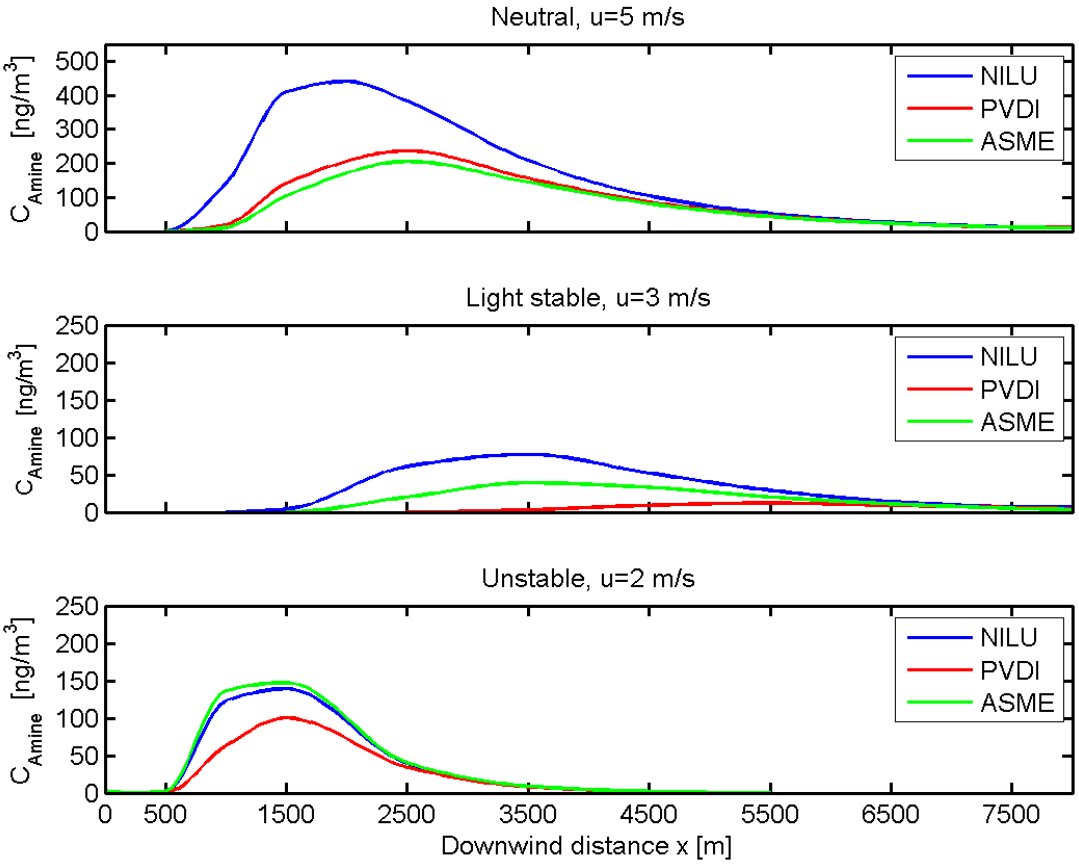

Figure S2: Sensitivity test of plume-rise parameterizations of this work ('NILU Plume', 'PVDI Plume', and 'ASME Plume') with a Gaussian plume model, showing ground-level concentrations in the centreline of the plume as a function of the downwind distance from the elevated point source. Three typical situations in the atmospheric boundary layer are considered: neutral case with wind speed u = 5 m s^{-1} (top part), moderately (light) stable case with u = 3 m s^{-1} (middle part), and unstable case with u = 2 m s^{-1} (bottom part).

a) **b)**

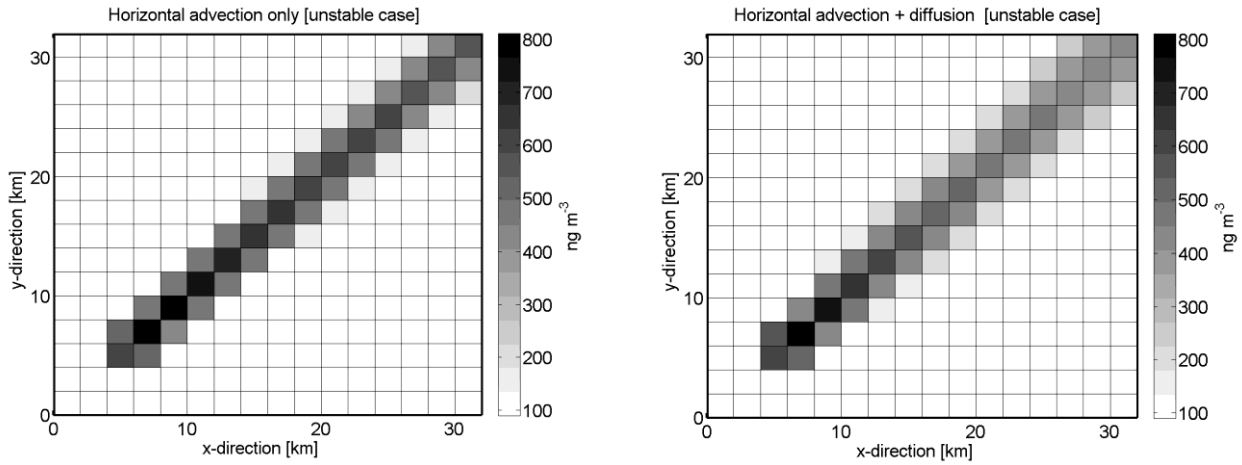

Figure S3: Horizontal dispersion test with EPISODE on 2-km resolution scale for unstable conditions: a) ground-level concentrations (in ng m^{-3}) when only horizontal advection is operative, and b) ground-level concentrations when horizontal advection and horizontal diffusion are operative. Volume source (2000 × 2000 × 90 m^3) with emission of 1 g s^{-1} was placed in the cell at x = 5 km, y = 5 km. In the test, ambient temperature gradient was dT/dz = -0.02 K m^{-1}, mixing layer height was 1000 m, and horizontal wind from 45 degrees was constant with wind speed u = 3 m s^{-1}.

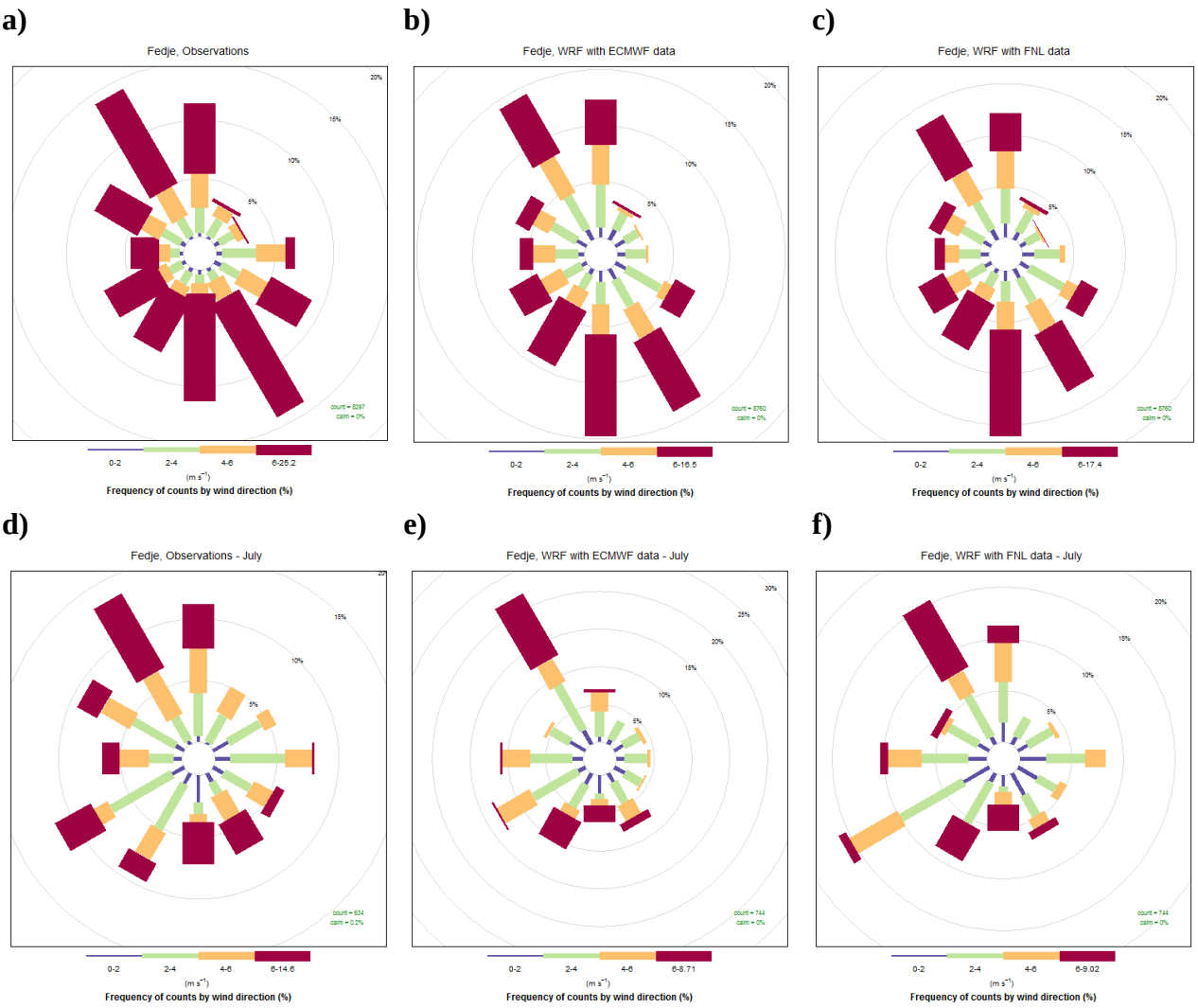

Figure S4: Comparison of wind roses for the year 2007 and for July 2007 at Fedje station [60.78ºN; 4.72ºE; 19 m a.s.l.]: a) annual wind rose based on observations, b) annual wind rose based on WRF model with ECMWF met data, c) annual wind rose based on WRF model with NCEP FNL data, d) July wind rose based on observation, e) July wind rose based on WRF model with ECMWF, and f) July wind rose based on WRF model with NCEP FNL data.

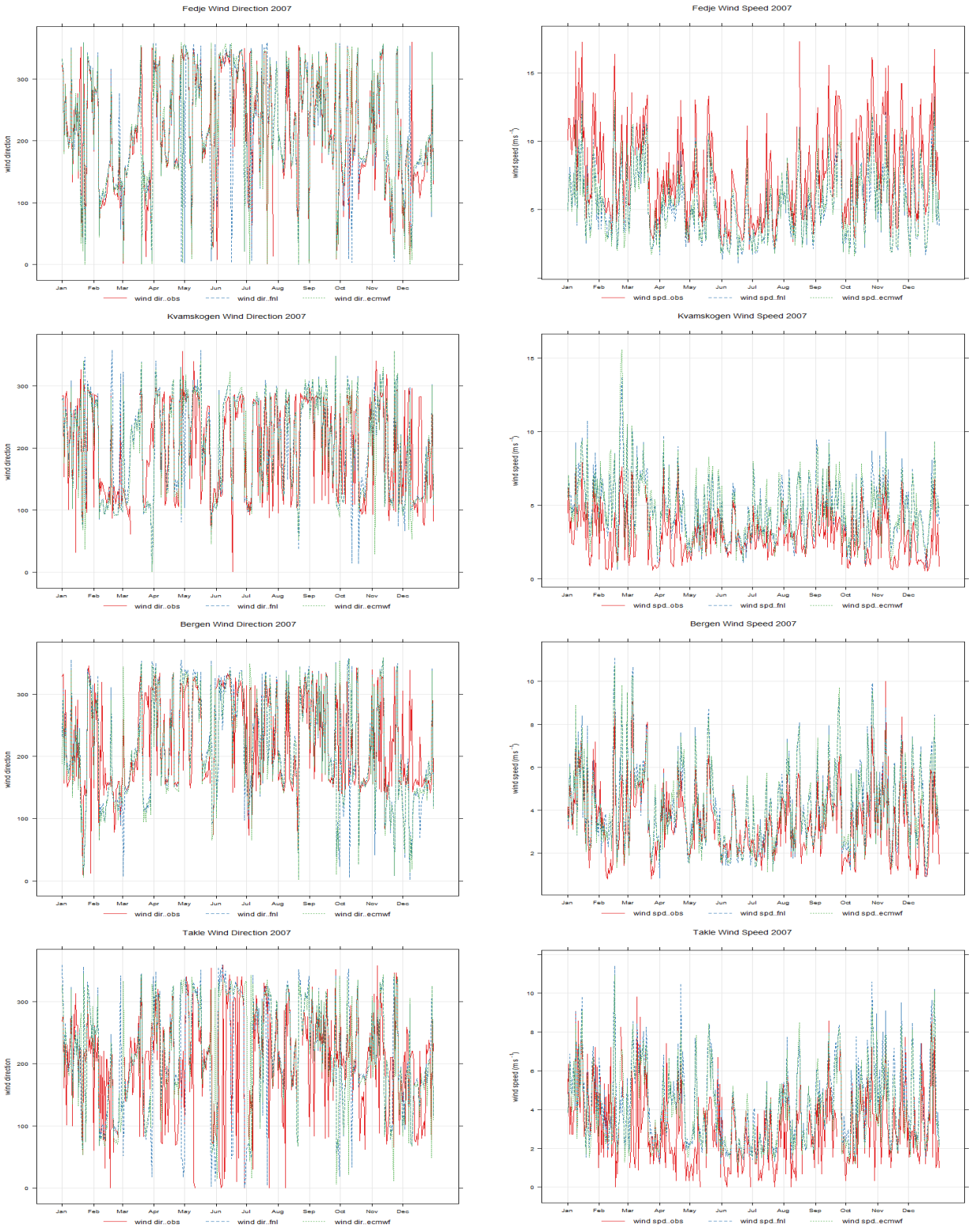

Figure S5: Comparison of wind direction (left column) and wind speed (right column) time series for 2007 at Fedje, Kvamskogen, Bergen and Takle based on daily average intervals from observation (red line) and WRF model with ECMWF data (green dashed line) and WRF model with NCEP FNL data (blue dashed line).

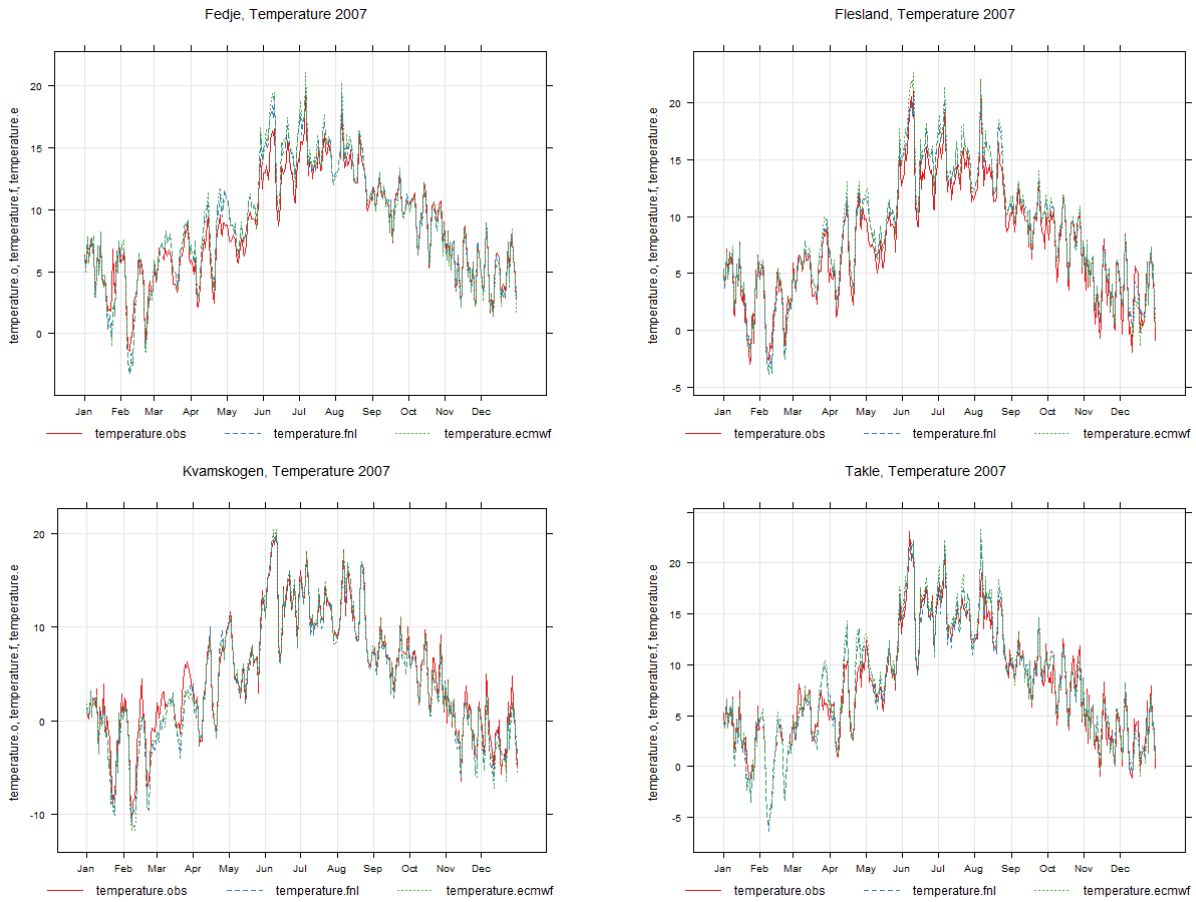

Figure S6: Comparison of temperature time series for 2007 at Fedje, Flesland, Kvamskogen, and Takle based on daily average intervals from observation (red line), WRF model with ECMWF data (green dashed line) and WRF model with NCEP FNL data (blue dashed line).

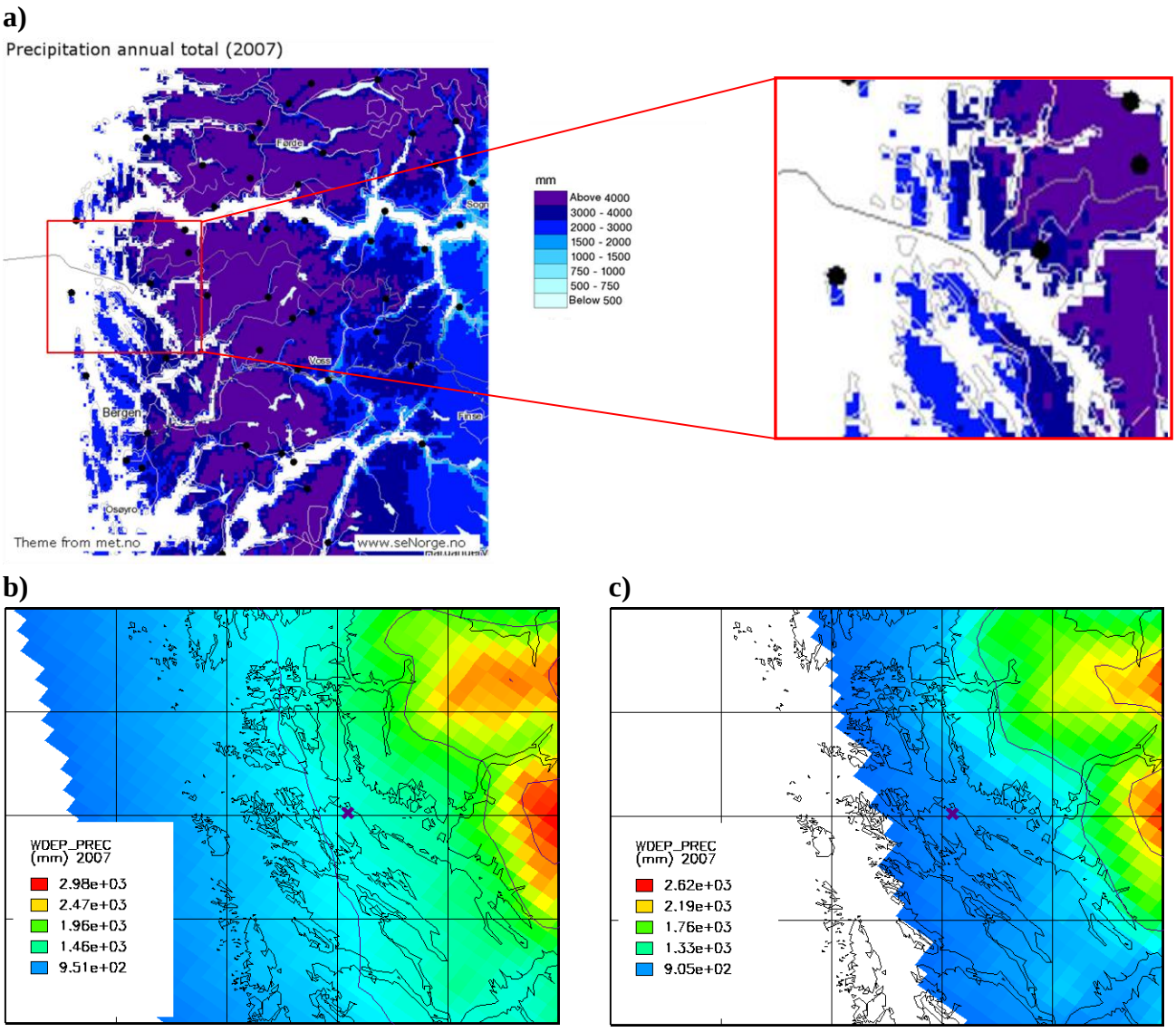

Figure S7: Total annual precipitation amount (as rain and snow) in 2007: a) map generated based on precipitation measurements from the Norwegian Meteorological Institute (available at http://noserge.no), red square showing approximate extend of the study area, a zoom into the area is shown to the right, b) precipitation map based on WRF model with ECMWF met data, and c) precipitation map based on WRF model with NCEP FNL data. The modelled total precipitation amount with NCEP FNL met data is uniformly 10-15% lower than with ECMWF met data.

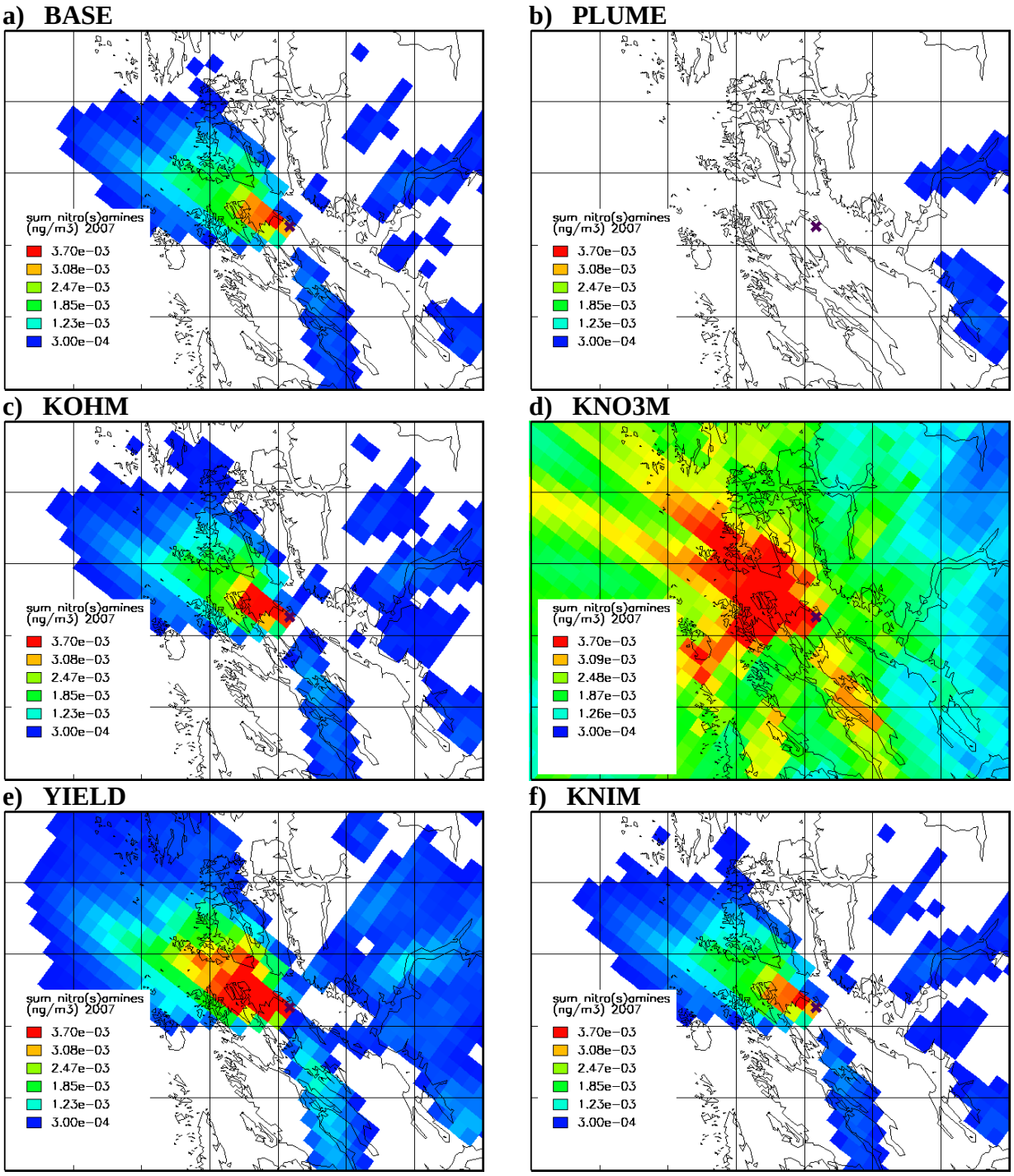

Figure S8: Continued.

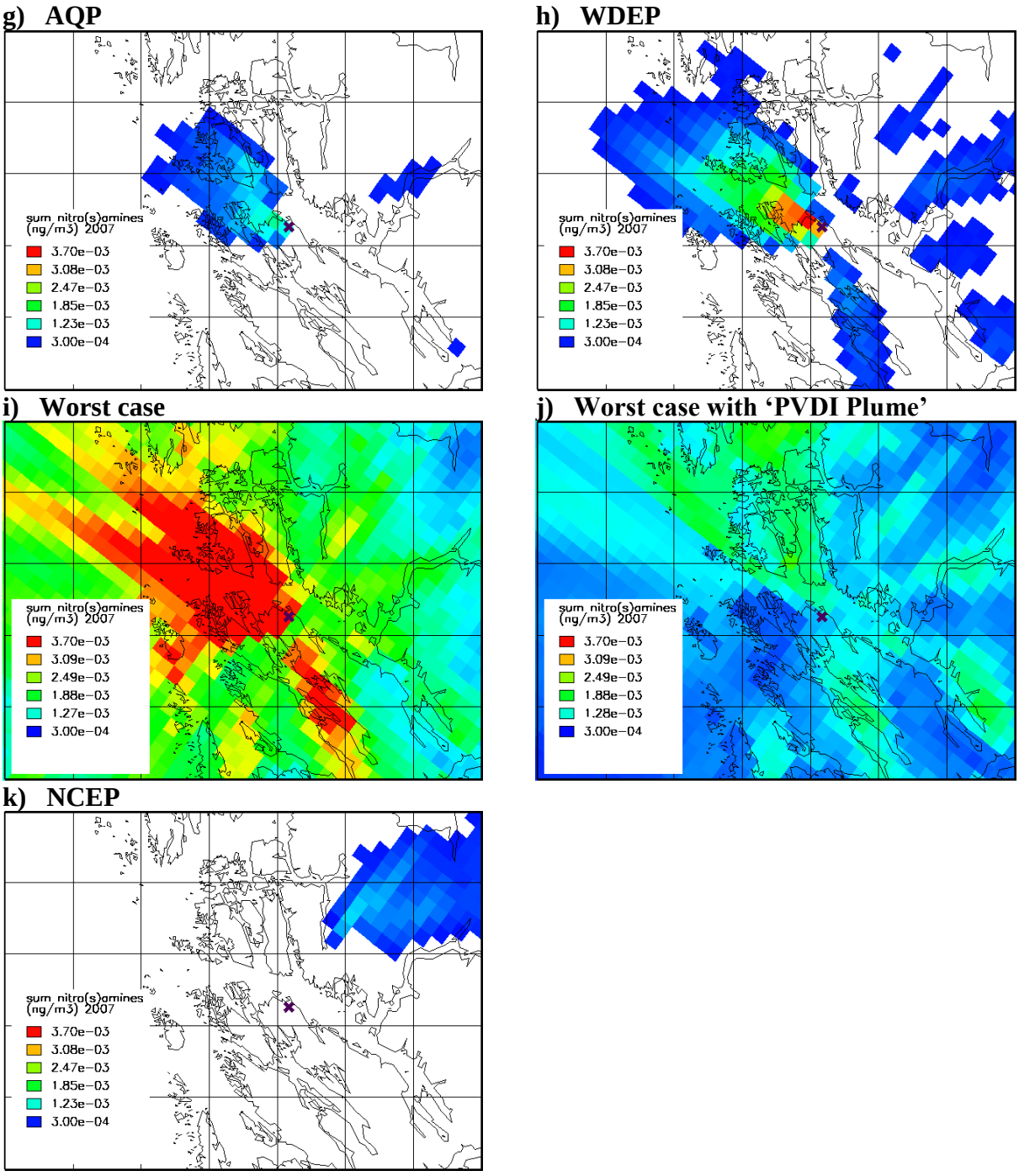

Figure S8: Air concentration of the sum of nitrosamines and nitramines (in ng m^{-3}) at ground level. Spatial distribution of the annual average (year 2007) computed by WRF-EMEP in a) case BASE, b) case PLUME, c) case KOHM, d) case KNO3M, e) case YIELD, f) case KNIM, g) case AQP, h) case WDEP, i) Worst case, j) Worst case with 'PVDI Plume', and k) Baseline case using NCEP FNL met data. Values below the smallest legend entry are not shown. Plots have the same concentration scale with an upper cut-off at 3.7×10^{-3} ng m^{-3} for better comparability. The location of CCP Mongstad is marked by a purple X. The grid cells divided by black lines illustrate an extent of 10x10 km^2.

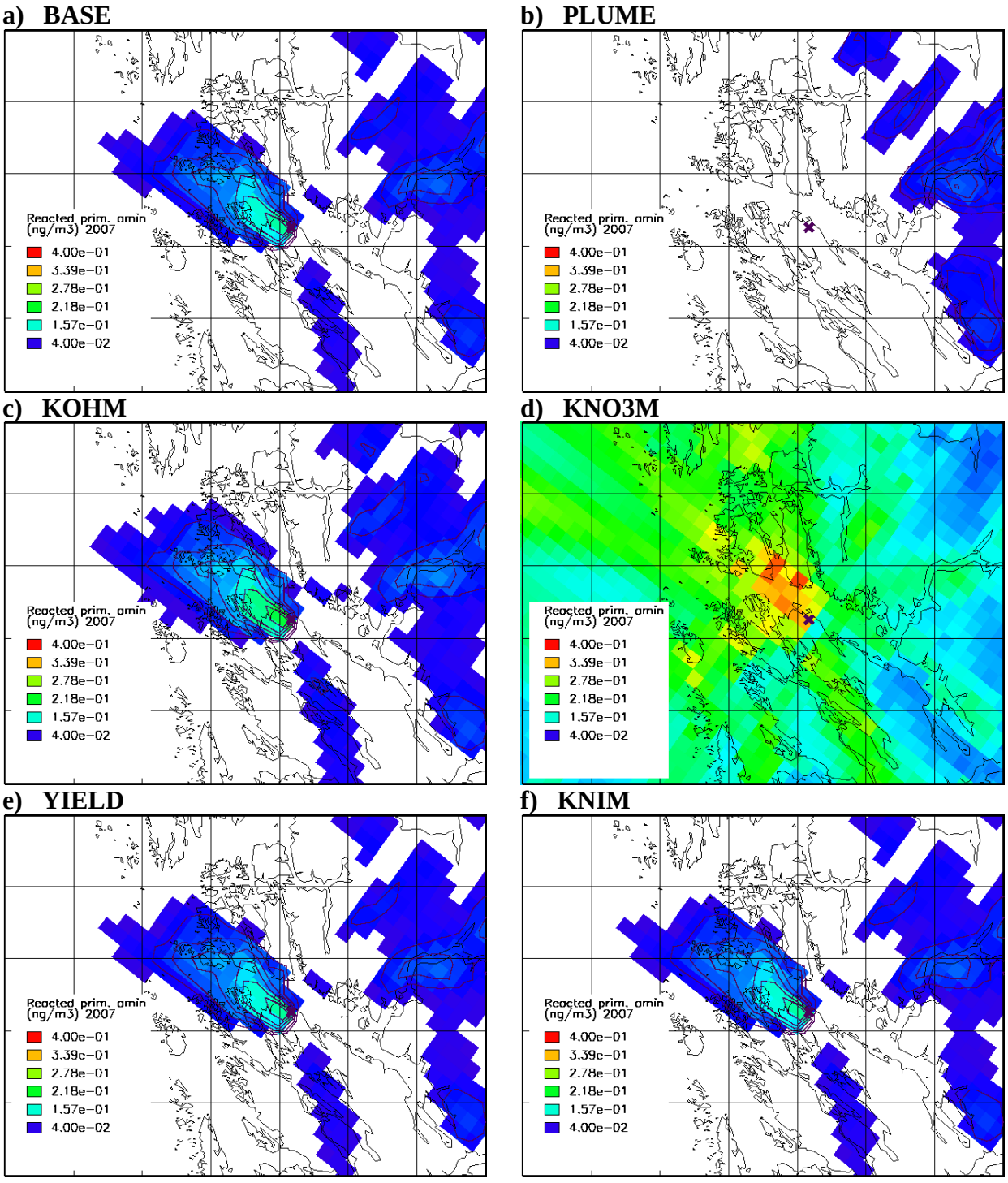

Figure S9: Continued.

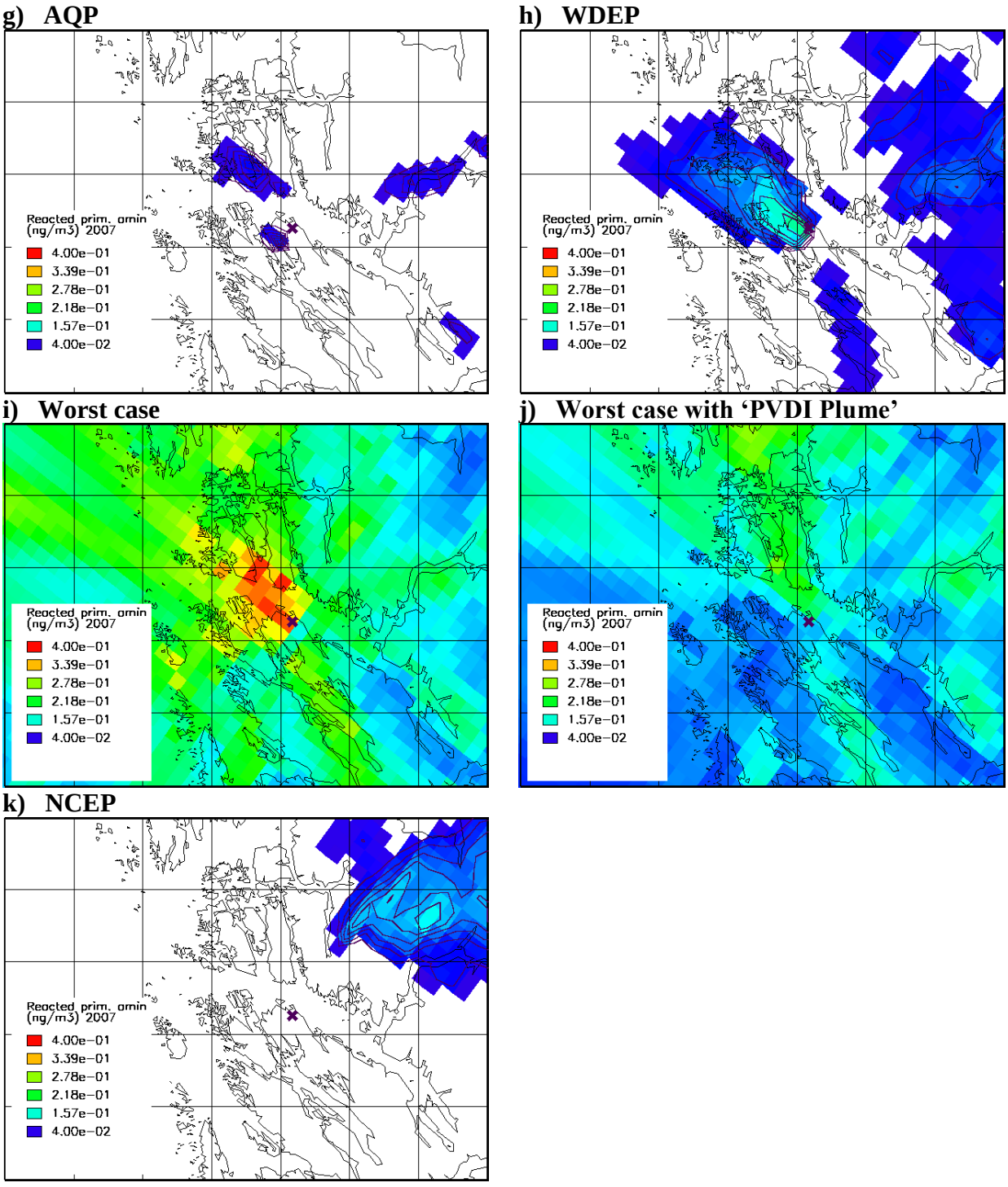

Figure S9: Reacted amount of MEA at ground-level on annual average (year 2007) expressed as concentration difference (in ng m^{-3}) for: a) case BASE, b) case PLUME, c) case KOHM, d) case KNO3M, e) case YIELD, f) case KNIM, g) case AQP, h) case WDEP, i) Worst case, j) Worst case with 'PVDI Plume', and k) Baseline case using NCEP FNL met data. All plots have the same scale. Values below the smallest legend entry are not shown. The location of CCP Mongstad is marked by a purple X. The grid cells divided by black lines illustrate an extent of 10x10 km^2.

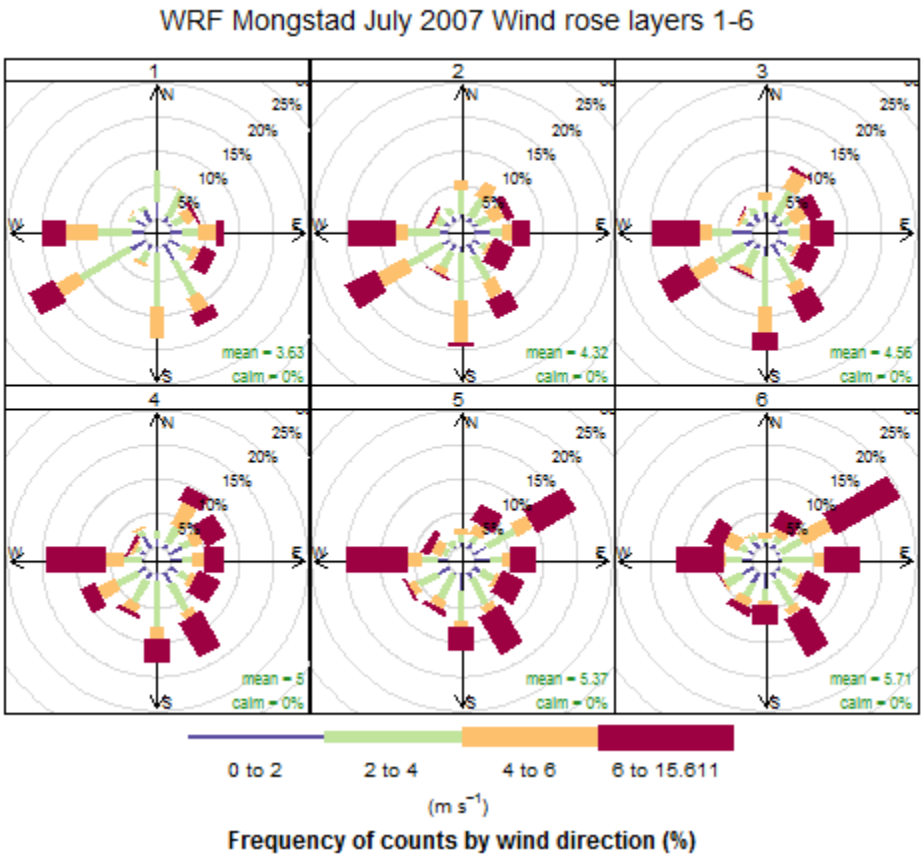

Figure S10: Wind roses for the six lowermost layers in the WRF model (up to ~1117 m) at location CCP Mongstad for July 2007, based on ECMWF met data. In layer 3 (184-324 m) highest wind speeds occur for wind directions 100°-150° and around 250°. On average, a certain shift in the wind speed and direction from the lowermost layer up to the top (sixth) layer is notable, with less wind coming from south-west - and more coming from north-east - in the upper layers.

References

ASME, American Society of Mechanical Engineers, Recommended Guide for the Prediction of the Dispersion of Airborne Effluents, 2nd ed., ASME, New York, U.S.A., 1973.

Briggs, G. A.: Some recent analyses of plume rise observation, In: Proceedings of the Second International Clean Air Congress, Ed. H. M. Englund and W. T. Berry, Academic Press, Washington, U.S.A., pp. 1029-1032, 1971.

Kuenen, J., Denier van der Gon, H., Visschedijk, A., and van der Brugh, H.: High resolution European emission inventory for the years 2003 - 2007, TNO report TNO-060-UT-2011-00588, Utrecht, Netherlands, 2011.

Pregger, T. and Friedrich, R., Effective pollutant emission heights for atmospheric transport modelling based on real-world information, Environmental Pollution, 157, 552-560, 2009.

Schaap, M., Hendriks, C., Kranenburg, R., Cuvelier, C., Thunis, P., Fagerli, H., Simpson, D., Schulz, M., Colette, A., Terrenoire, E., Bessagnet, B., Rouïl, L., Stern, R., and Graff, A.: Performance of European chemistry transport models as function of horizontal resolution, http://www.unece.org/fileadmin/DAM/env/documents/2012/air/EMEP_36th/N_10_Performance_of_European_chemistry_transport_models_as_function_of_horizontal_resolution_14_sep_2012.pdf, 2012 (last access: 23 June 2014)

Seinfeld, J. H. and Pandis, S. N., Ch. 18.5 Plume Rise, In: Atmospheric Chemistry and Physics, From Air Pollution to Climate Change, pp. 931-933, John Wiley & Sons Inc., New York, U.S.A., 1998.

Simpson, D., Benedictow, A., Berge, H., Bergström, R., Emberson, L. D., Fagerli, H., Flechard, C. R., Hayman, G. D., Gauss, M., Jonson, J. E., Jenkin, M. E., Nyíri, A., Richter, C., Semeena, V. S., Tsyro, S., Tuovinen, J.-P., Valdebenito, Á., and Wind, P.: The EMEP MSC-W chemical transport model – technical description, Atmos. Chem. Phys., 12, 7825-7865, 2012.

Slørdal, L. H., Solberg, S., and Walker, S. E.: The Urban Air Dispersion Model EPISODE applied in AirQUIS2003. Technical description, Norwegian Institute for Air Research, Kjeller, NILU TR 12/03, 2003.

US EPA: Estimation Programs Interface Suite for Microsoft Windows, v 4.00, United States Environmental Protection Agency, Washington, DC, USA, available at: http://www.epa.gov/opptintr/exposure/pubs/episuite.htm (last access: 23 June 2014), 2012.

VDI: Ausbreitung von Luftverunreinigungen in der Atmosphäre; Berechnung der Abgasfahnenüberhöhung. (Dispersion of air pollutants in the atmosphere; determination of plume rise) 1985-06 (German/English), Kommission Reinhaltung der Luft (KRdL) im VDI und DIN - Normenausschuss, 1985, available at: http://www.vdi.de/technik/fachthemen/reinhaltung-der-luft/, (last access: 23 June 2014)

Walker S. E., Slørdal L. H., Guerreiro C., Gram F., and Grønskei, K. E.: Air Pollution exposure monitoring and estimation. Part II. Model evaluation and population exposure, J. Environ. Monit, 1, 321-326, 1999.

Yiannoukas, S., Morale, G., Williams, R., and Johnson, A.: Deposition and soil transport modelling of components from postcombustion amine-based CO2 capture, Report for Gassnova SF. Det Norske Veritas Ltd, UK, Report No. PP011015, London, U.K.. available at: http://www.gassnova.no/no/Documents/Depositionandsoiltransportmodelling_DNV.pdf, (last access: 23 June 2014), 2011.